

Article

A Study on the Pyrolysis Behavior and Product Evolution of Typical Wood Biomass to Hydrogen-Rich Gas Catalyzed by the Ni-Fe/HZSM-5 Catalyst

Xueqin Li ^{1,2}, Yan Lu ¹, Peng Liu ^{1,*}, Zhiwei Wang ^{3,4}, Taoli Huhe ¹, Zhuo Chen ⁵, Youqing Wu ² and Tingzhou Lei ^{1,*}

¹ Changzhou Key Laboratory of Biomass Green, Safe & High Value Utilization Technology, National-Local Joint Engineering Research Center of Biomass Refining and High-Quality Utilization, Institute of Urban and Rural Mining, Changzhou University, Changzhou 213164, China; lxq8889@126.com (X.L.); luyan6667@163.com (Y.L.); hhtaoli@cczu.edu.cn (T.H.)

² Department of Chemical Engineering for Energy Resources, School of Resources and Environmental Engineering, East China University of Science and Technology, Shanghai 200237, China; wyq@ecust.edu.cn

³ School of Environmental Engineering, Henan University of Technology, Zhengzhou 450001, China; zw.wang@gaut.edu.cn

⁴ Institute for Carbon Neutrality, Henan University of Technology, Zhengzhou 450001, China

⁵ School of Management and Economics, North China University of Water Resources and Electric Power, Zhengzhou 450046, China; chenzhuo@ncwu.edu.cn

* Correspondence: liupeng@cczu.edu.cn (P.L.); ltz@cczu.edu.cn or china_newenergy@163.com (T.L.)

Abstract: The thermo-chemical conversion of biomass wastes is a practical approach for the value-added reclamation of bioenergy in large quantities, and pyrolysis plays a core role in this process. In this work, poplar (PR) and cedar (CR) were used as staple wood biomasses to investigate the apparent kinetics of TG/DTG at different heating rates. Secondly, miscellaneous wood chips (MWC), in which PR and CR were mixed in equal proportion, were subjected to comprehensive investigations on their pyrolysis behavior and product evolution in a fixed bed reactor with pyrolysis temperature, catalyst, and the flow rate H₂O steam as influencing factors. The results demonstrated that both PR and CR underwent three consecutive pyrolysis stages, the TG/DTG curves shifted to higher temperatures, and the peak temperature intervals also enhanced as the heating rate increased. The kinetic compensation effect expression and apparent reaction kinetic model of CR and PR pyrolysis were obtained based on the law of mass action and the Arrhenius equation; the reaction kinetic parameter averages of E_a and A of its were almost the same, which were about 72.38 kJ/mol and 72.36 kJ/mol and 1147.11 min⁻¹ and 1144.39 min⁻¹, respectively. The high temperature was beneficial for the promotion of the pyrolysis of biomass, increased pyrolysis gas yield, and reduced tar yield. This process was strengthened in the presence of the catalyst, thus significantly increasing the yield of hydrogen-rich gas to 117.9 mL/g_{biomass}. It was observed that H₂O steam was the most effective activator for providing a hydrogen source for the whole reaction process, promoted the reaction to proceed in the opposite direction of H₂O steam participation, and was beneficial to the production of H₂ and other hydrocarbons. In particular, when the flow rate of H₂O steam was 1 mL/min, the gas yield and hydrogen conversion were 76.94% and 15.90%, and the H₂/CO was 2.07. The yields of H₂, CO, and CO₂ in the gas formation were significantly increased to 107.35 mL/g_{biomass}, 53.70 mL/g_{biomass}, and 99.31 mL/g_{biomass}, respectively. Therefore, H₂ was the most dominant species among gas products, followed by C-O bond-containing species, which provides a method for the production of hydrogen-rich gas and also provides ideas for compensating or partially replacing the fossil raw material for hydrogen production.

Keywords: wood biomass; Ni-Fe/HZSM-5 catalyst; pyrolysis behavior; products evolution; gaseous products



Citation: Li, X.; Lu, Y.; Liu, P.; Wang, Z.; Huhe, T.; Chen, Z.; Wu, Y.; Lei, T. A Study on the Pyrolysis Behavior and Product Evolution of Typical Wood Biomass to Hydrogen-Rich Gas Catalyzed by the Ni-Fe/HZSM-5 Catalyst. *Catalysts* **2024**, *14*, 200. <https://doi.org/10.3390/catal14030200>

Academic Editor: Anna Maria Raspolli Galletti

Received: 1 February 2024

Revised: 8 March 2024

Accepted: 14 March 2024

Published: 19 March 2024



Copyright: © 2024 by the authors. Licensee MDPI, Basel, Switzerland. This article is an open access article distributed under the terms and conditions of the Creative Commons Attribution (CC BY) license (<https://creativecommons.org/licenses/by/4.0/>).

1. Introduction

Pyrolysis technology plays a significant role in the sectors of petrochemicals, chemicals, and energy and is responsible for the production of various energy products [1]. In response to the changing global energy security situation and the increasing emphasis on environmental protection, enterprises in the petrochemical, chemical, and energy production sectors are actively exploring new pyrolysis technologies. As one of the important thermochemical conversion technologies, biomass pyrolysis refers to the process of heating and degrading biomass raw materials to combustible gas, liquid bio-oil, and solid biochar under anaerobic or anoxic conditions [2]. In the process of pyrolysis, biomass raw materials would incur a series of physical (heat transfer and material transfer during the heating process, etc.) and chemical changes (primary, secondary, and even multi-level chemical reactions) by controlling the conditions of the pyrolysis process (raw material types and compositions, reaction temperatures, heating rate, residence times and reactor types, etc.), resulting in different types of products [3]. The technology and principle of the traditional pyrolysis of biomass are shown in Figure 1, and the research status of pyrolysis and gasification reactors nationally and globally is shown in Table 1. Among them, the fixed bed reactor is an internal thermal coupling process, which can be divided into updraft, downdraft, and transverse fixed bed reactors according to the movement direction of airflow in the furnace. That is, gas is used as a heat carrier to make contact with raw materials and, in turn, provide heat. The structure is relatively simple and has many advantages, such as a wide adaptability of raw materials, simple manufacturing, low costs, few moving parts, simple operation, and the high thermal efficiency of the system. However, fixed bed pyrolysis has certain requirements on the particle size, ash content, and ash melting point of biomass, and to maintain the autothermal reaction system, air should be used as a gasifying agent. Thus, the resulting gas is easy to dilute with N_2 and CO_2 , reducing the content of effective components such as H_2 and CO , and the content of by-products such as tar is high, which is not conducive to the production of hydrogen-rich gas. At the same time, according to the structure, the pyrolysis process of the fluidized bed is divided into a bubbling fluidized bed gasifier, circulating fluidized bed gasifier, airflow bed gasifier, conical fluidized bed gasifier, etc., which have the advantages of high heat and mass transfer efficiency, high production capacity, and uniform reaction temperature. However, the dust entrainment is serious, the gas–solid residence time is short, and the carbon conversion rate is low. In addition, the pyrolysis process of the airflow bed uses oxygen as a gasifying agent, and the operating environment of high temperature and high pressure is dangerous. Therefore, it is urgent to solve the various problems caused by controlling the sub-processes of biomass pyrolysis and gasification. It is also urgent to reform and solve the various problems that arise in different chemical reactions caused by the mutual shackles of thermodynamics and kinetics. In particular, tar is an important by-product; it is difficult to achieve selective regulation and the efficient removal of the reaction process.

By analyzing the thermogravimetric (TGA), derivative thermogravimetric (DTG), and pyrolysis characteristics of biomass, we may explore whether hydrogen-rich gas can be prepared by the catalytic pyrolysis of biomass. The TGA and DTG data obtained from thermogravimetric balances are widely used to determine the intrinsic kinetics of pyrolysis. Kinetic parameters such as the apparent activation energy and pre-exponential factor are primarily estimated by either the model-based method or the model-free method [4]. Tan et al. [5] found an increase in temperature was found to elevate the CO , CH_4 , and monocyclic aromatic hydrocarbon content, whereas it decreased the contents of phenols, acids, aldehydes, and other oxygenates. In addition, the catalytic pyrolysis process effectively inhibited the production of acids, phenols, and furans in the liquid.

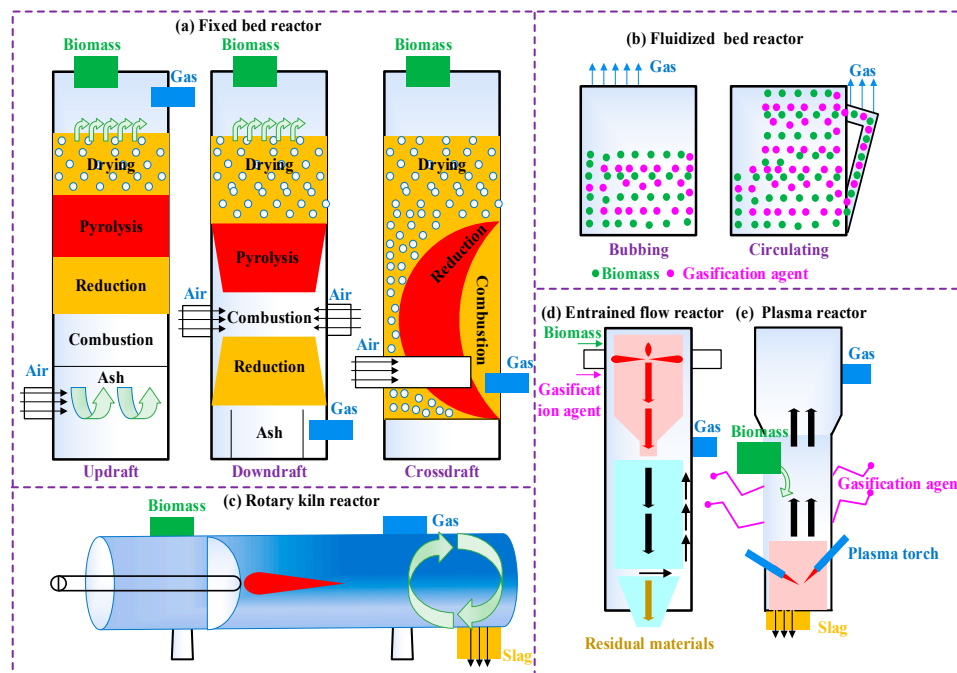


Figure 1. Schematic view of different types of reactors.

Table 1. Research status of pyrolysis/gasification reactor.

Research Organization	Pyrolytic Technique	Country	Sale (kg/h)
Dynamotive	Fluidized bed	Canada	1500
Red Arrom/Emsyn	Circulating fluidized bed	America	1250
Red Arrom/Emsyn	Circulating fluidized bed	America	1000
ENEL/Emsyn	Circulating fluidized bed	Italy	625
BTC/kara	Rotating cone	Netherlands	200
Uniom Feboea/Waterloo	Fluidized bed	Spain	200
Ensym	Circulating fluidized bed	Canada	100
BTC	Rotating cone	Netherlands	50
University of Hamburg	Fluidized bed	Germany	50
University of Laval	Vacuum fluidized bed	Canada	50
NREL	Ablation rotating cone	America	30
RTI	Fluidized bed	Canada	30
VET/Ensym	Circulating fluidized bed	Finland	30
CRES	Circulating fluidized bed	Greece	20
University of Waterloo	Fluidized bed	Canada	4

Catalytic pyrolysis is an efficient method of biomass thermal conversion. Under the action of a catalyst, pyrolysis products can be cracked into short-chain intermediate products by the dehydration or decarboxylation of long-chain bio-oil molecules and inhibit the occurrence of secondary cracking reactions; thus, high-quality target products can be obtained by directional conversion [6]. Recently, catalytic pyrolysis has attracted substantial research and commercialization attention, with over 15,000 journal articles and patents published in the past decade alone. Wang et al. [7] overviewed the catalytic reaction routes, reaction types, and key steps involved in the selective preparation of various important products from lignocellulose and put forward the rational design methods of active and robust heterogeneous catalysts. Eliseo et al. [8] analyze the main kinetic features of biomass pyrolysis, devolatilization, and the gas phase reactions of the released species. Wang et al. [9] comprehensively reviewed recent advances in both the fundamental studies and technological applications of biomass pyrolysis. Therefore, the overall pyrolysis process of biomass can be considered the decomposition of polymer chains in biomass

macromolecules to produce condensable volatiles (bio-oil), no condensable gases, and biochar via externally supplied heat under an inert atmosphere. But the outcomes of biomass pyrolysis are heavily dependent on its reaction conditions. However, at present, the research on the pyrolysis mechanism of biomass pyrolysis is mostly based on the structure of biomass raw materials and pyrolysis products to deduce the possible reaction path in the process of pyrolysis or to speculate the possible evolution path of product functional groups by a method of theoretical calculation. More importantly, obtaining high-quality hydrogen-rich gas by improving and optimizing reaction conditions not only serves as one of the important paths toward the development of biomass pyrolysis technology, but it also provides an important theoretical basis for promoting the utilization of biomass pyrolysis gas.

Based on the structure of the chemicals of biomass and their components and relying on thermogravimetric behavior and pyrolysis kinetics, this study explored and optimized the process of the catalytic pyrolysis of wood biomass to hydrogen-rich gas in a fixed-bed reactor with pyrolysis temperature, catalysts, and H₂O steam as influencing factors; this was to determine the reaction path and mechanism of catalytic pyrolysis and provides a theoretical basis for the pyrolysis process of biomass. This study also paves the way for a greener and more sustainable low-carbon future.

2. Results and Discussion

2.1. Pyrolysis Kinetics of Wood Biomass

2.1.1. TG/DTG Analysis

The TG and corresponding DTG curves of PR and CR at the heating rates of 10, 20, 30, and 40 °C/min are shown in Figure 2. The higher the peak value, the faster the reaction rate at this temperature. As shown in Figure 2, it is quite clear that the whole decomposition process can be categorized into three successive stages, i.e., drying, rapid pyrolysis, and carbonization. In the drying stage (before 200 °C), the biomass samples were preheated, and the external moisture gradually evaporated and was removed from light volatile matter. Since biomass is a complex polymer, structural evolutions, like depolymerization, reorganization, and glass transition, would take place in this stage, that is, the modification of raw biomass materials [10]. The rapid pyrolysis stage (200–600 °C) was the major weight loss stage, in which a great number of volatile substances were continuously generated due to the thermal decompositions of weak bonds between cellulose and hemicellulose as well as the linkages between lignin monomers. Additionally, it was observed that the temperature ranges during the pyrolysis of PR and CR were similar, which was 200–550 °C at different heating rates, which is the maximum decomposition rate of both hemicellulose and cellulose. In particular, more components of CR and PR were decomposed or transformed before 400 °C. The maximum mass loss rate (~50%) was about 330–390 °C, and the corresponding maximum weight loss temperatures were located at 365 °C and 370 °C, respectively, with a heating rate of 30 °C/min. So, the order of their thermal stability was CR > PR. In other words, the range of the pyrolysis interval for PR was similar to that of CR, indicating that a similar pyrolysis reaction was shown in the pyrolysis process of wood biomass. In the carbonization stage (600–900 °C), the rest of the lignin fractions with high bond energies tended to aggregate, forming char structures (fixed carbon) and presenting slow variations in weight loss. Among the three major components in biomass, lignin is the only polymer that has an aromatic structure, including various branches and strengthened bonds [11], which gives it high thermal stability. Thus, thermal decomposition takes place over a wider temperature range and covers the whole pyrolysis process. Meanwhile, the TG/DTG curves were roughly close to a straight line until the end of the pyrolysis reaction.

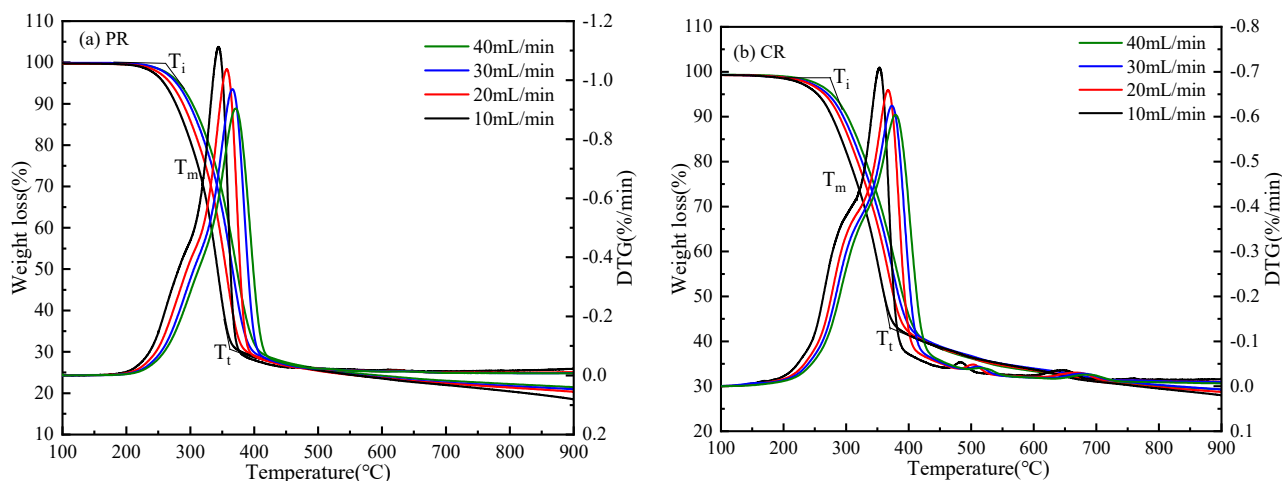


Figure 2. TG/DTG curve of wood biomass at different heating rates.

The DTG peak shows the overall degradation rate of all reactions combined [12]. It was also observed from Figure 2 that DTG curves showed similar variation trends in addition to the acceleration of pyrolysis rates with an increase in heating rates. In comparison, there was a difference in the position and height of the peak, which is consistent with the study of Garima et al. [13]. As the heating rate increased from 10 °C/min to 40 °C/min, the initial and final temperatures all shifted slightly to a higher temperature range, and the maximum weight loss temperature and pyrolysis interval also increased. The above situation might be attributed to (1) the increase in heat rate during pyrolysis leading to the decrease in heat transfer efficiency or (2) the higher heating rate stimulated by augmented thermal energy promoting the proceeding pyrolysis reactions, thus increasing the maximum value of the pyrolysis rate. The pyrolysis characteristic parameters of PR and CR at four heating rates are shown in Table 2. Among them are $x = 0.99$, $n = 1$, and $R = 8.31$. Therefore, the pyrolysis of wood biomass is mainly a process of carbon enrichment, and the depolarity functional group of organic components and the pyrolysis reaction are facilitated at a higher heating rate. The pyrolysis of cellulose, hemicellulose, and lignin is interactive [14]. The existence of lignin inhibits the thermal polymerization of polysaccharides in cellulose, promotes the formation of medium- and low-molecular-weight products in cellulose, and reduces the content of char. The existence of cellulose inhibits the formation of char in lignin and promotes the formation of lignin derivatives. In comparison, the reaction between cellulose and lignin is more obvious in the process of pyrolysis.

Table 2. Pyrolysis characteristic parameters of PR and CR at different heating rates.

Sample	β (mL/min)	m_0 (mg)	m (mg)	m_∞ (mg)	t (min)	T (K)	RT
PR	10	12.66	1.41	1.27	146.00	1123.15	9337.87
	20	12.11	1.61	1.52	104.50	1123.50	9340.78
	30	12.69	1.69	1.62	92.18	1123.33	9339.32
	40	12.41	1.63	1.56	85.76	1123.33	9339.32
CR	10	17.41	3.31	3.15	142.00	1123.15	9337.87
	20	15.98	3.08	2.97	104.50	1123.50	9340.78
	30	16.16	3.18	3.06	92.18	1123.33	9339.32
	40	16.07	3.15	3.05	85.76	1123.33	9339.32

2.1.2. Analysis of Apparent Kinetics

The kinetic parameters, including the activation energy (E_a) and preexponential factor (A), of two wood biomasses were calculated according to the law of mass action and the Arrhenius equation based on TG analysis. The E_a and A data are shown in Table 3. It can be seen in Table 3 that there are some differences in E_a and A at different heating rates. In general, the increase in E_a is accompanied by the increase in A . However, as the shape of the curve in the TG method is related to the heating rate and other test conditions, it is necessary to introduce the corresponding kinetic compensation effect. According to the research of relevant scholars [15], there is a relationship between kinetic parameters A and E_a as follows: $\ln(A) = aE_a + b$. Furthermore, the data points in Table 3 are linearly fitted to obtain the expression of the kinetic compensation effect of CR and PR pyrolysis, as shown in Equations (1) and (2).

$$\ln(A) = 0.09583E_a + 0.12230 \quad (1)$$

$$\ln(A) = 0.09548E_a - 0.1470 \quad (2)$$

Table 3. Kinetic parameters of biomass pyrolysis under different heating rates.

β (mL/min)	PR		CR	
	E_a (kJ/mol)	A (min ⁻¹)	E_a (kJ/mol)	A (min ⁻¹)
10	73.89	1341.81	73.04	1237.76
20	72.22	1144.56	72.27	1150.18
30	71.69	1091.38	72.44	1169.72
40	71.63	1084.02	71.77	1099.88

The E_a obtained at different heating rates was averaged, and the A was obtained by using the kinetic compensation effect expression. The apparent reaction kinetic model of wood biomass was obtained, as shown in Equations (3) and (4).

$$\frac{dx}{dT} = \frac{1147.11}{\beta} \exp\left(-\frac{72,380}{8.314T}\right) (1-x)^n \quad (3)$$

$$\frac{dx}{dT} = \frac{1144.39}{\beta} \exp\left(-\frac{72,360}{8.314T}\right) (1-x)^n \quad (4)$$

It was obvious from Table 4 that there was little difference in the pyrolysis kinetic parameters of the two wood biomasses, and the E_a of their pyrolysis reactions was about 72 kJ/mol. This was mainly due to the small difference in the composition of cellulose, hemicellulose, and lignin, which led to little difference in the thermal reaction path, transformation direction, and difficulty degree of transformation in the heated state. This slight difference was mainly due to the different degrees of decomposition of the three components at different temperature levels and the different durations of pyrolysis with the continuous increase in temperature. Specifically, cellulose produced a small amount of carbon after rapid pyrolysis between 325 °C and 375 °C, lignin slowly pyrolyzed to form more carbon between 250 °C and 500 °C, and hemicellulose decomposed rapidly between 225 °C and 325 °C [16]. The pyrolysis of three components produced different products, which promoted/inhibited each other. Therefore, the complex heat and mass transfer in the pyrolysis process and many factors lead to the difference in the kinetic behavior of the pyrolysis process of biomass. Additionally, the greater the E_a , the more difficult the pyrolysis reaction at the same temperature [17]. The E_a difference between CR and PR was very small, indicating that the difficulty of pyrolysis at the same temperature was the same. At the same time, other types of raw materials with higher E_a need to consume more external energy to achieve the same conversion effect under the same conditions. Therefore, it is necessary to optimize the pyrolysis reaction conditions, improve the heat and mass

transfer conditions of the pyrolysis process, and grasp the pyrolysis reaction path to obtain specific target products.

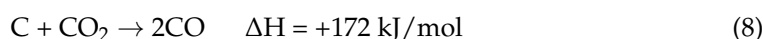
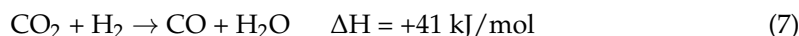
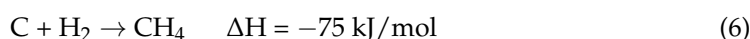
Table 4. Reaction kinetic parameters of pyrolysis of wood biomass.

Sample	Ea (kJ/mol)	A (min ⁻¹)
CR	72.38	1147.11
PR	72.36	1144.39

2.2. Effect of Pyrolysis Temperature on the Product Distribution from Catalytic Pyrolysis of MWC

2.2.1. Product Distribution and Release Rate of Pyrolysis Gas

Under the action of the Ni-Fe/HZSM-5 catalyst, the heating rate of 20 °C /min rose from 200 °C to 900 °C and was kept at this temperature for 30 min to explore the main product distribution law of the pyrolysis of MWC. The reaction formula for the catalytic pyrolysis of MWC is Equation (5). Figure 3 exhibits the released law analysis of gases from the catalytic pyrolysis of MWC at 200–900 °C. The analysis showed that H₂ was the most dominant gaseous product during the pyrolysis process; in addition, the gaseous products also comprised some small molecule gases, such as CO, CO₂, and CH₄. The effect mechanism of pyrolysis temperature on the release rate of each component was different. In particular, when the pyrolysis temperature reached 700 °C, the H₂ release rate reached the maximum (14.79 mL/min). This was because continuous heating promoted the bond-breaking transformation of macromolecules and strengthened the ability of hydrogen evolution. With the continued increase in temperature, the release rate of H₂ began to decrease, which was due to the complex reforming reaction (Equations (6)–(8)) between gases [18], indicating that the reaction before 700 °C was the process of releasing H₂ by the catalytic pyrolysis of MWC and the consumption process of H₂ in the reaction system occurred after 700 °C. Correspondingly, the release rate of CH₄ reached its maximum at 500 °C, which is beneficial to promote the effective cracking of intermediate products to achieve the best effect of hydrogen release. With the continued increase in temperature, the release rate of CH₄ began to decrease until it reached an equilibrium, indicating that the catalytic pyrolysis of MWC before 500 °C produced CH₄, and the reduction reaction of hydrogen and C to produce CH₄ (Equation (6)) occurred after 500 °C. When the CH₄ release rate began to equalize, the reduction reaction of CO₂ and H₂ (Equation (7)) and the gasification reaction of carbon deposition (Equation (8)) became the main reactions. The release rates of CO and CO₂ reached the highest at 400 °C, which were 14.41 mL/min and 23.56 mL/min, respectively, indicating that the maximum loss of the catalytic pyrolysis of MWC was delayed from 365 °C to 400 °C under the action of Ni-Fe/HZSM-5 catalyst.



The product distribution of the catalytic pyrolysis of MWC at different pyrolysis temperatures is shown in Figure 3b. The analysis showed that the gas yield increased to the maximum (51.22%) as the temperature increased from 400 °C to 700 °C. When the temperature continuously increased to 800 °C, the gas yield decreased obviously, which was mainly because the high temperature not only promoted the catalytic pyrolysis of MWC but also promoted the secondary cracking of by-products and the intermolecular polymerization of pyrolysis gas [19,20]. Thus, the highest tar yield was obtained at 800 °C (37.5%). When the temperature was further increased to 900 °C, the yield of char and tar decreased obviously, and the gas yield increased, indicating that the high temperature promoted the cracking of macromolecular substances, and the main reaction was the tar

cracking/reforming reaction [21]. Significantly, the tar yield appeared in the lowest range between 600 °C and 700 °C, the char yield showed a gradual downward trend and was 16.09% at 700 °C, and the total gas yield was 117.9 mL/g_{biomass} at this same temperature. Therefore, the pyrolysis temperature is an important factor in reducing tar yield and increasing gas yield.

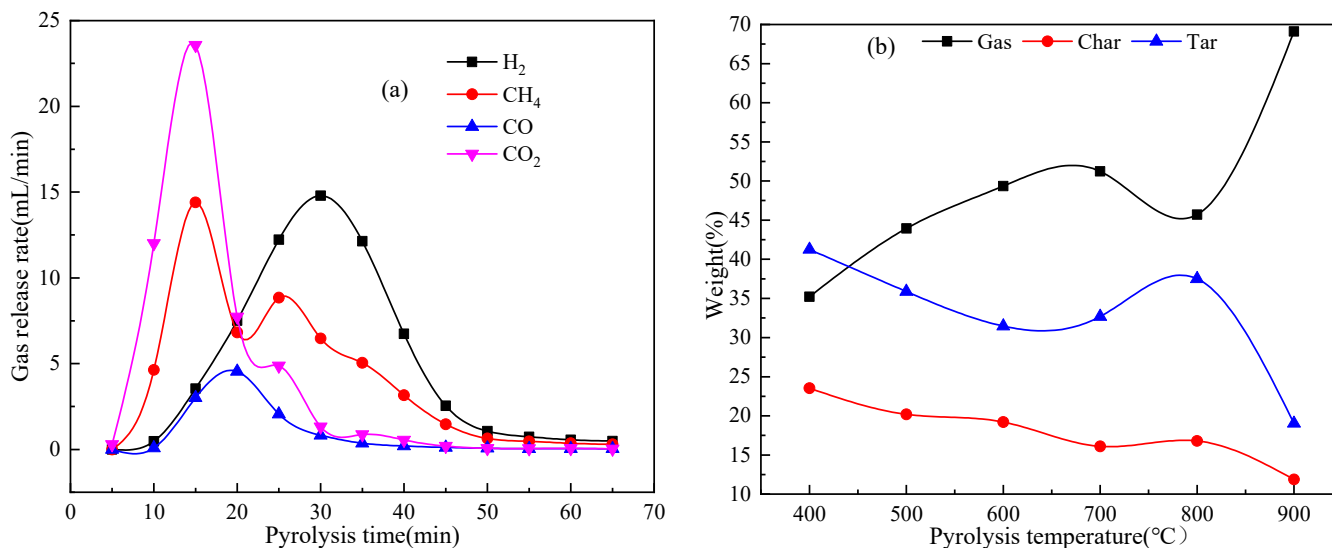


Figure 3. Effect of pyrolysis temperature on the release rate (a) and distribution of pyrolysis products (b).

2.2.2. Formation Process and Composition Distribution of Tar

The ion chromatography of tar and the serial numbers of corresponding substances from the catalytic pyrolysis of MWC at 400–900 °C are shown in Figure 4 and Table S1. The distribution of liquid products at different temperatures is shown in Table 5. From the distribution of compounds in tar composition, the composition is the same between 400 °C and 800 °C, mainly including aldehydes (AL), acids (AC), alcohols (ALc), ketones (KE), phenols (PH), furans (FU), esters (ES), and a small number of hydrocarbons. However, the content of the same substance varied greatly at different temperatures. At 400 °C, the AC substances were mainly acetic acid (6.99%), and the KE substances were acetone, butanone, pentanone, and their derivatives, with a content of 70.27%. The AL substances included succinaldehyde, furfural, carboxylic aldehyde, and their derivatives, with a content of 4.42%. The ALc substances included butanediol, methanol, alcohol, and their derivatives, with a content of 12.25%. The PH substances included methoxy, vinyl phenol, and their derivatives, with a content of 1.04%. The FU substances were acetyl furan benzofurans and their derivatives, with a content of 1.22%. The ES substances were phenyl carbamates, butyrolactone, and their derivatives, with a content of 2.69%. The ALk substances were propane derivatives, with a content of 1.13%. Furfural, 5-hydroxymethylfurfural, and acetic acid were the main products in the pyrolysis of hemicellulose, while vinyl phenol and L-glucan are representative products in the pyrolysis of lignin and cellulose [22], respectively. Therefore, the three components in MWC had different degrees of pyrolysis at ≤400 °C.

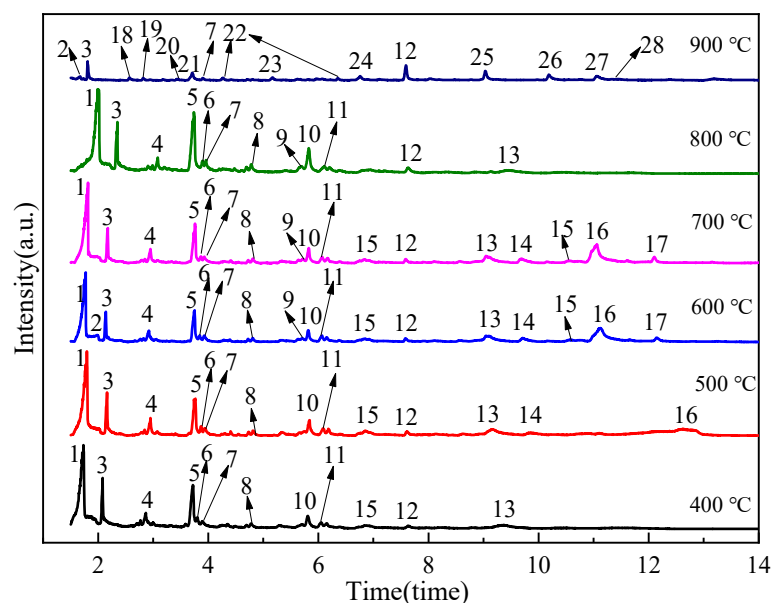


Figure 4. Effect of pyrolysis temperature on the liquid products of catalytic pyrolysis of MWC.

Table 5. Distribution of liquid products by the catalytic pyrolysis of MWC at different pyrolysis temperatures.

Type	Name	Percent Proportion (%)					
		400 °C	500 °C	600 °C	700 °C	800 °C	900 °C
AC	Acetic acid	3.96	36.01	24.50	23.74	42.91	
	Acetic acid, (acetyloxy)-						1.61
	Propanoic acid			2.61		2.67	2.44
	Dodecanoic acid, 3-hydroxy-	3.03	4.42	1.05	2.71		
KE	2-Propanone, 1-hydroxy-	66.28	6.53	3.30	5.04	5.53	9.86
	1-Hydroxy-2-butanone	0.90	0.99		0.70		2.40
	1-Hydroxy-2-pentanone						1.80
	2-Cyclopenten-1-one	2.32	2.65	2.02	1.65	2.07	1.62
	2-Propanone, 1-(acetyloxy)-	0.77	3.74				6.15
	2-Cyclopenten-1-one, 2-hydroxy-						
	2-Cyclopenten-1-one, 2-hydroxy-3-methyl-						6.16
AL	Succindialdehyde						1.40
	3-Furaldehyde	1.19	10.43	7.68	9.06	1.74	
	2-Furancarboxaldehyde, 5-methyl-	3.23		2.50	3.13	6.91	
	Furfural						9.03
	5-Hydroxymethylfurfural		20.32	15.26	16.82		
ALc	2,3-Butanediol	4.24	4.16	33.02	3.38	2.49	
	2-Furanmethanol	2.40	1.95	1.47	1.18	2.91	
	Creosol						12.27
	2-Propyl-tetrahydropyran-3-ol	5.60	6.06	6.00	64.83	4.75	

Table 5. Cont.

Type	Name	Percent Proportion (%)					
		400 °C	500 °C	600 °C	700 °C	800 °C	900 °C
ALk	Propanal, 2,3-dihydroxy-, (S)-	1.13			1.34		
	Phenol, 2-methoxy-	1.04	1.04	0.77	0.91	2.25	14.06
PH	Phenol, 4-ethyl-2-methoxy-						9.39
	Phenol, 2,6-dimethoxy-			2.03	1.76		
	Phenol, 2-methoxy-5-(1-propenyl)-, (E)-						3.13
	Phenol, 2-methoxy-4-(1-propenyl)-						9.25
	2-Methoxy-4-vinylphenol						9.43
FU	Ethanone, 1-(2-furanyl)-	1.22	0.91	0.72	0.79	1.46	
	Benzofuran, 2,3-dihydro-		2.09	2.25	2.65		
ES	Carbamic acid, methyl-, phenyl ester	1.19		0.90	0.90	2.01	
	Butyrolactone	1.49	18.60	1.55	1.55	1.90	

With the pyrolysis temperature increase to 500 °C, the contents of AC, AL, FU, and ES substances increased significantly to 40.43%, 20.32%, 3%, and 18.60%, respectively. The KE substances content decreased significantly to 13.91%, and the contents of ALk, ALc, and PH substances were not significantly changed, indicating that the appropriate increase in temperature promoted the complete pyrolysis of three components from MWC. When the pyrolysis temperature increased to 600 °C, the AC substance content decreased to 25.55%. In particular, the acetic acid content decreased significantly, and propionic acid appeared; the contents of KE, AL, and ES substances further decreased to 5.31%, 25.45%, and 2.45%, respectively. But the contents of PH and ES substances increased significantly to 2.79% and 20.32%, indicating that an increasing temperature was beneficial to increasing the length of the carbon chain and promoting the pyrolysis of KE substances to produce gas. However, when the pyrolysis temperature reached 700 °C, the vinyl phenol appeared in PH substances, and the content of ALc substances increased significantly to 69.39%; the content of ALc substances also increased by 18.4%, indicating that 700 °C was beneficial for the complete pyrolysis of lignin. Furthermore, when the pyrolysis temperature was further increased to 800 °C, the AC substances content increased again, indicating that the high temperature promoted the polymerization and depolymerization of small oxygen-containing molecular substances to form acids. The dehydration of alcohols and decarboxylation of carboxylic acids were typical deoxidization reactions to produce H₂O and CO₂ [23], significantly decreasing the contents of ALc and AL substances to 10.16% and 8.65%. There are some macromolecular oxygen-containing substances in AL, PH, and KE substances at 900 °C, which may be due to the ketonization initiated by the catalyst; that is, the conversion of carboxyl and acid into ketones leads to a significant increase in the content of KE substances [24–26]. The distribution law of the catalytic pyrolysis of biomass is summarized in Figure 5; the increase in temperature promotes the formation of phenols and alcohols. The ketone compounds are not much affected by temperature, but the presence of ketones can effectively reduce the viscosity of tar. It can also reduce the thermal stability and chemical stability of tar, so it is necessary to inhibit the formation of ketones in the process of improving the pyrolysis of biomass.

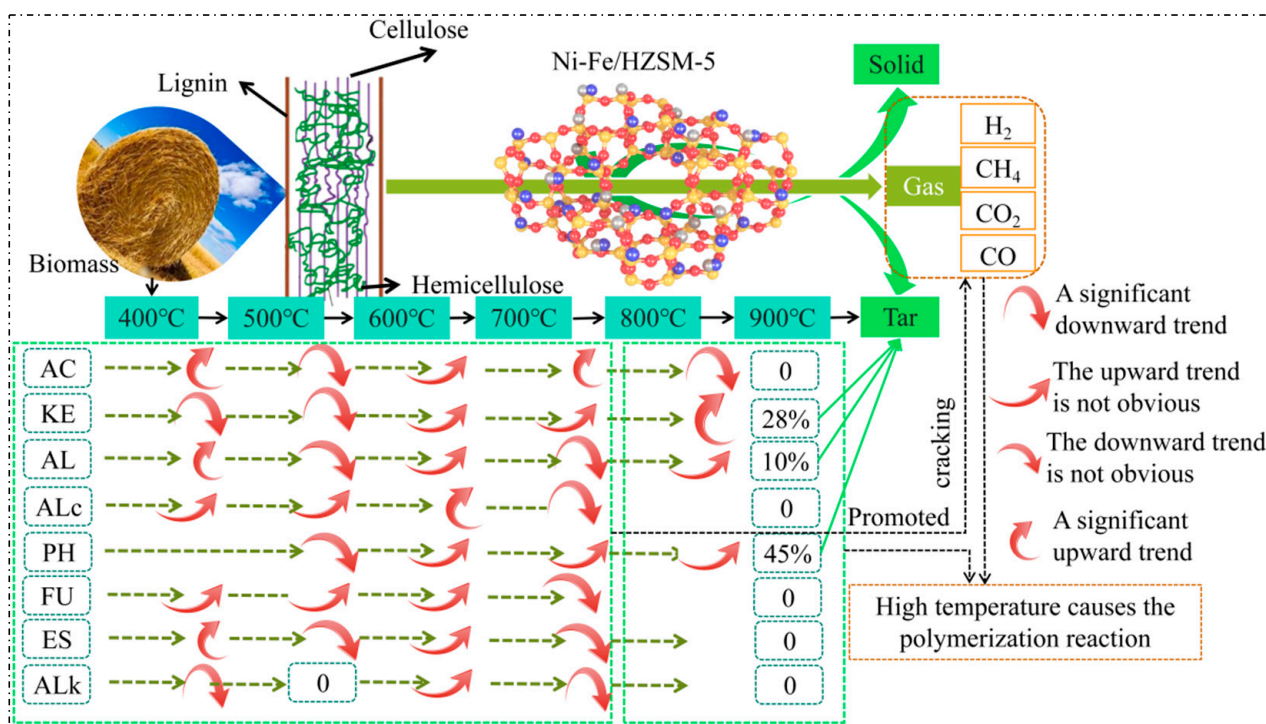


Figure 5. Product distribution of catalyzing pyrolysis of biomass.

2.3. Enhanced Catalytic Pyrolysis of Wood Biomass under H₂O Steam Atmosphere

The effect of H₂O steam and its flow rate (0.5 mL/min, 1 mL/min, 1.5 mL/min, 2 mL/min) on the catalytic pyrolysis of MWC was investigated. The product distribution and gas yield are shown in Figure 6. The analysis showed that the additional introduction of H₂O steam promoted the catalytic pyrolysis process of MWC. In particular, when the flow rate of H₂O steam increased to 1 mL/min, the gas yield and H conversion ratio increased obviously to 76.94%, 15.90%, and H₂/CO ratio to 2.07. In the gas production composition, the yields of H₂, CO, and CO₂ were significantly increased to 107.35 mL/g-biomass, 53.70 mL/g-biomass, and 99.31 mL/g-biomass, respectively. This indicated that the additional introduction of H₂O steam could provide a hydrogen source for the whole reaction process and significantly enhance the char gasification reaction (Equation (9)) and water vapor shift reaction (Equation (10)), which is beneficial to the production of H₂ and other hydrocarbons [27].

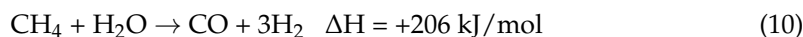


Figure 7 shows the release rate of main gases at different flow rates of H₂O steam. Obviously, as the flow rate of H₂O steam increased to 2 mL/min, the gas yield decreased, and the tar yield decreased to a certain extent and then began to maintain equilibrium. This was because the tar had a self-reforming reaction with H₂O and CO₂, indicating that the additional introduction of H₂O steam would shorten the residence time of tar-containing gas in the reforming reactor. Thus, the cracking/reforming reaction of tar was inhibited and consumed a lot of energy, which can be explained by Figure 8. As can be seen from Figure 8, the degree of carbon deposition on the surface of the catalyst increased with the increase in H₂O steam flow rate, indicating that too much H₂O steam reduced the conversion of tar, resulting in the accumulation of a large number of macromolecular substances to form carbon deposition and cover the surface of the catalyst. Therefore, the additional introduction of H₂O steam promotes the steam gasification reaction of char and water-gas change reaction but avoids the introduction of excessive H₂O steam.

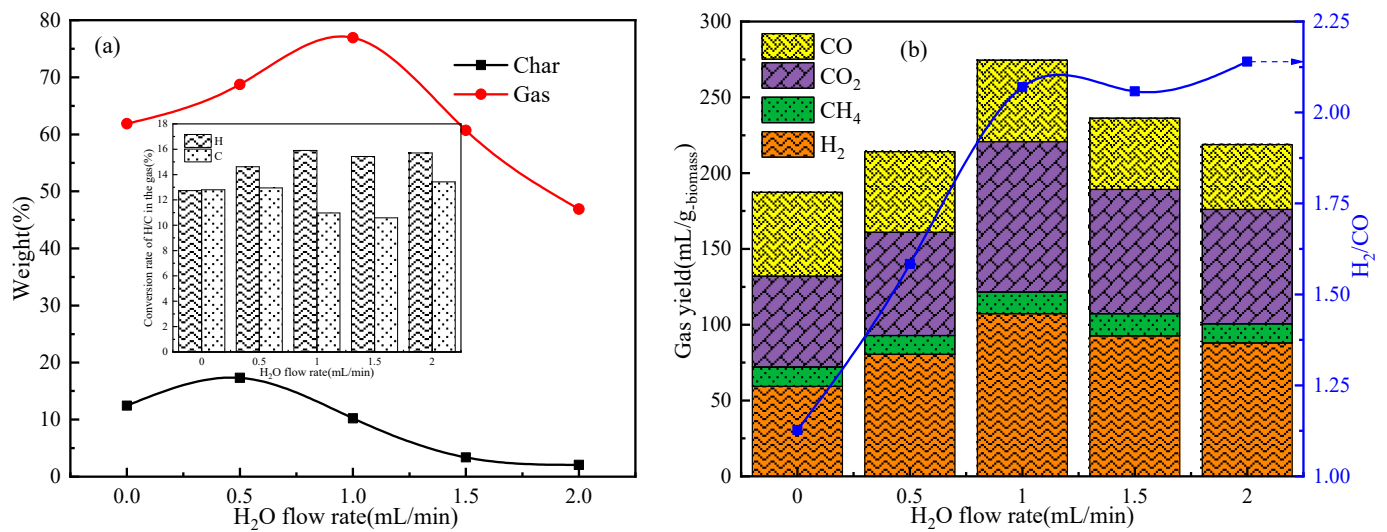


Figure 6. Effect of H₂O steam flow rate on the distribution of pyrolysis products of catalytic MWC, (a) distribution of pyrolysis product, (b) gas yield and H₂/CO.

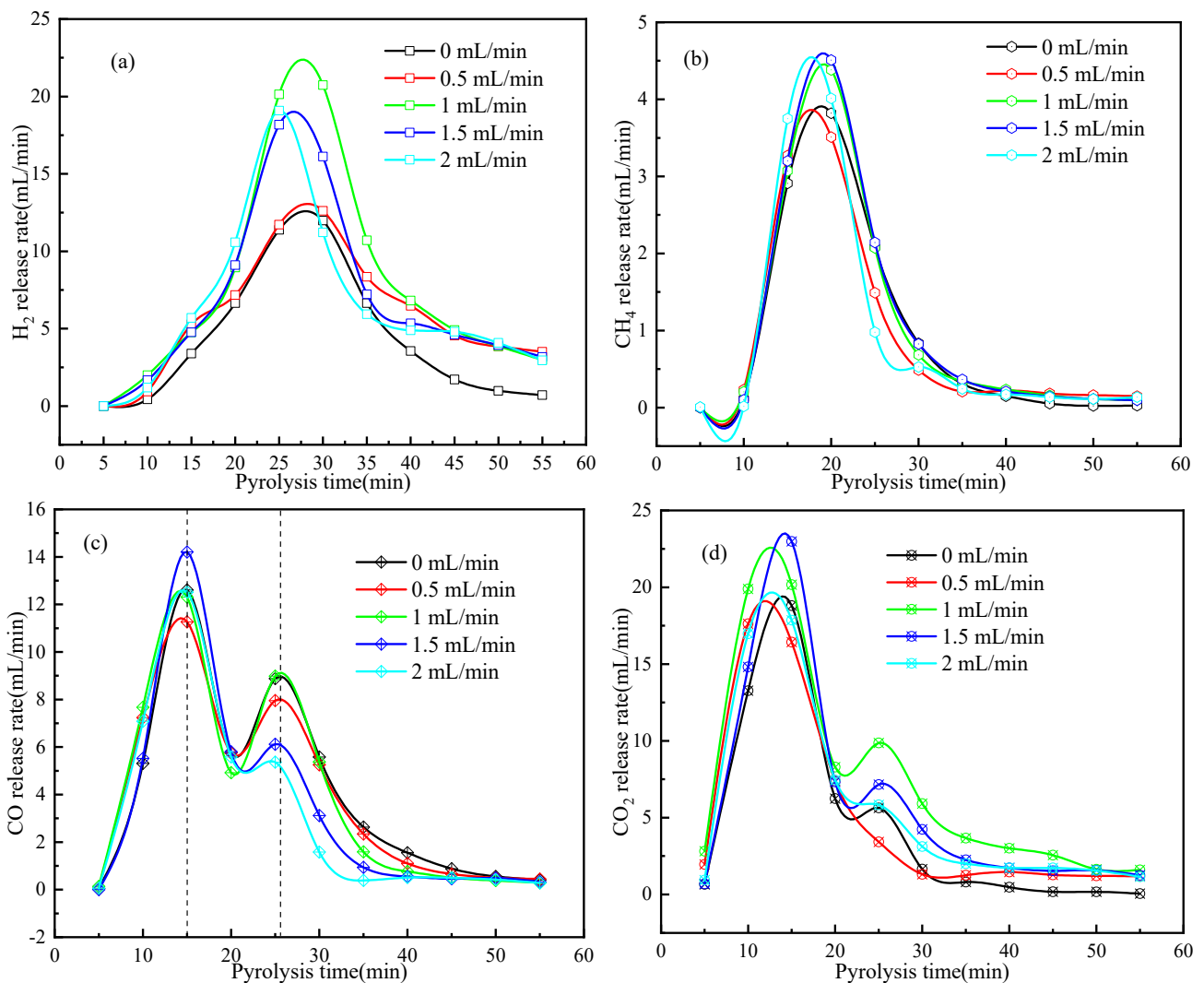


Figure 7. Effect of H₂O flow rate on the gas release from catalytic pyrolysis of MWC, (a) H₂ release rate, (b) CH₄ release rate, (c) CO release rate, and (d) CO₂ release rate.

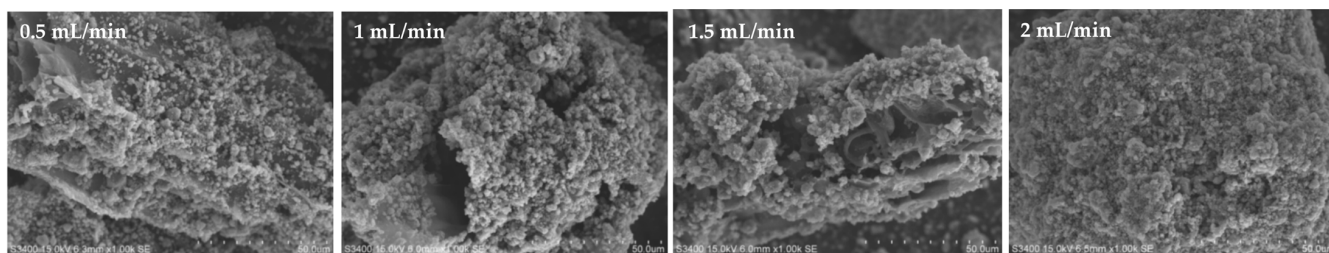


Figure 8. SEM of reacted catalysts by the catalytic pyrolysis of MWC at different H₂O steam flow rates.

Furthermore, the pore characteristics of the reacted catalyst at different flow rates were analyzed, as shown in Figure 9 and Table 6. Compared with fresh catalysts, the ring degree of the hysteresis loop from the N₂ adsorption/desorption curve of the reacted catalyst varied obviously at different flow rates of H₂O steam. The pore size varied greatly in the range of 0–5 nm. In addition, H₂O steam enlarged the specific surface area and pore volume of the catalyst in varying degrees. In particular, the pore characteristic of the reacted catalyst under 1 mL/min H₂O steam was better, which was consistent with the analysis of the experimental results.

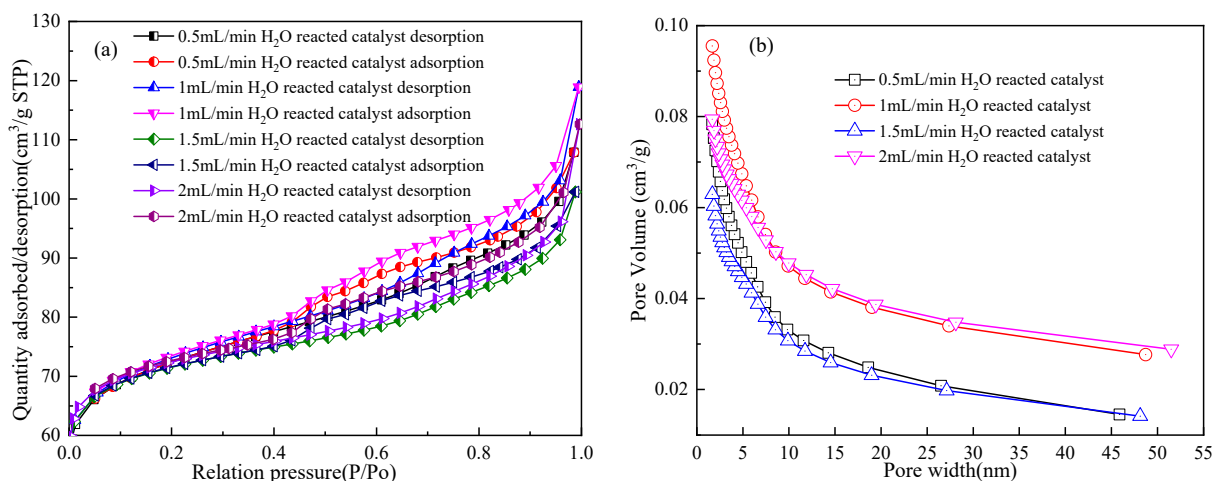


Figure 9. N₂ adsorption/desorption isotherms and pore distribution of reacted catalysts, (a) quantity adsorbed/desorption, and (b) distribution of pore volume.

Table 6. Effect of H₂O flow rate on the pore characteristics of catalyst.

Sample	BET Surface Area (m ² /g)	t-Plot Micropore Area (m ² /g)	Total Pore Volume (cm ³ /g)	Pore Size (nm)	Average Nanoparticle (nm)
Reacted catalyst under 0.5 mL/min H ₂ O	227.56	157.86	0.17	2.93	26.37
Reacted catalyst under 1 mL/min H ₂ O	229.30	157.15	0.18	3.21	26.17
Reacted catalyst under 1.5 mL/min H ₂ O	224.82	171.25	0.16	2.82	26.16
Reacted catalyst under 2 mL/min H ₂ O	224.35	174.34	0.17	3.11	26.74

Table 7 listed the related studies on the production of hydrogen-rich gas by the catalytic pyrolysis of biomass in recent years [27–40], in which the catalyst type, type of raw material, gas composition, and yield were taken as indicators. In contrast, in this study, the pyrolysis temperature and flow rate of H₂O steam had a great influence on the

catalytic pyrolysis law of wood biomass. In particular, a suitable temperature guarantees the complete conversion of wood biomass and catalyst stability, and the type of catalyst is the basis of the resistance to carbon deposition and hydrogen production by the directional pyrolysis of wood biomass. However, the residence time of pyrolysis gas is limited, and the contact condition between tar-containing gas and bed material is poor, leading to insufficient conversion of tar and polymerization to form heavy components, which affects the conversion and utilization efficiency of wood biomass. At the same time, biomass tar often contain a variety of oxygenated compounds, which can compromise their usefulness as a fuel [41]. Therefore, effectively controlling the formation of tar from the pyrolysis source and prolonging the contact time between tar-containing gas and bed material is an important condition to achieve effective tar removal.

Table 7. Comparison of the effects of catalytic pyrolysis of biomass.

Catalyst	Raw Material	Temperature (°C)	Gas Production Composition (vol%)			
			H ₂	CH ₄	CO	CO ₂
40%wtCaCO ₃	Rice straw	750	11.8		14.5	15
K ₂ CO ₃ /Ni-Al ₂ O ₃	Coking coal	560	61.4	0	1.9	36.6
Ni-based catalyst biocarbon	Apricot pit	850	88.74	9.15		
	Corn straw	800	34.53	10.71		30.37
Dolomite		650	79.1			
	Pine	900	70.5			
Ni-Mo/Al ₂ O ₃	Sawdust	600	52.82	3.8	33.68	8.63
	SiO ₂	Sawdust	600	0.45	9.31	3.65
Ni-Al ₂ O ₃ -Ca	Pine	500	0.04	0.36	3.27	3.38
	Pine		31.31	1.8	49.83	16.4
Ni-based catalyst	Wood biomass	700	46.03	0.79	39.03	14.15
	Cellulose		34.67	1.08	47.36	16.83
Ni-CaO catalyst	Pine	750	60.23	6.74	18.44	13.18
	1.8Ni/Al ₂ O ₃	Pine	900	29.78	15.55	39.97
W-Ni0.65	Beech wood	600	0.58	0.9	10	16.6
RM800-40%Fe ₂ O ₃	Corn straw	900	22.98	29.8	36.6	10.6
5%SiO ₂	Wheat straw	600	20.7	7.89	25.86	45.6
BFeCo	Bamboo	850	32.6	7.96	27.97	28.76

3. Materials and Method

3.1. Raw Materials

Two kinds of feedstock (poplar, PR, and cedar, CR) from the wood processing plant were crushed and ground to obtain particles less than <40 mm by a grinder and stored in a desiccator for analysis of apparent kinetics. The proximate analysis was monitored according to standard methods shown in our previous paper [42,43]. The elemental analyzer (Elementar Vario Micro Cube, Shanghai, China) was used to analyze elements of C, H, N, and S, and the O element was calculated by mass difference. Cellulose, hemicellulose, and lignin contents were determined by the classical method proposed by Van Soest [44]. The results of proximate analysis, ultimate analysis, and fiber analysis of two wood biomass samples are shown in Table 8. The mixture of PR and CR in equal proportion was used as the samples of the catalytic pyrolysis experiment, which is called miscellaneous wood chips (MWC).

The catalyst was synthesized according to the method shown in our previous paper [45], used HZSM-5 (H-type zeolite molecular sieve-5) with a SiO₂/Al₂O₃ ratio of 25 as support, and impregnated by a 0.17 mol/L solution of Ni(NO₃)₂·6H₂O, and the Ni loading was 8 wt.%. Fe(NO₃)₃·9H₂O was used as a precursor of the promoter Fe, and the loading of Fe was 4 wt.% (relative to the amount of Ni). After impregnation, the mixture was dried overnight, followed by calcination at 550 °C for 3 h, marked Ni-Fe/HZSM-5. The surface properties and pore structures of catalysts were determined by surface area and porosity instrument (Tristar II 3020, MICRO cube, USA), shown in Table 9. The micromorphology of

catalysts was analyzed by scanning electron microscope (SUPRA55, ZEISS, Oberkochen, Germany), shown in Figure 10. Interaction of Ni and Fe was characterized by XPS technique (K-Alpha, Thermo Scientific, Waltham, MA, USA) with the excitation source of Al K α ray, as shown in Figure 10.

Table 8. Proximate, ultimate, and fiber analyses of PR and CR.

Sample	Proximate Analysis/%				QG (MJ/Kg)		
	M _{ad}	A _{ad}	V _{ad}	FC _{ad}			
PR	9.70	1.30	83.65	16.35	16.62		
CR	10.57	5.35	80.04	19.96	16.40		
Sample	Ultimate analysis (dry)/%						
	N	C	H	S	O #	H/C	O/C
PR	0.48	53.51	7.27	0.04	38.70	1.63	0.54
CR	0.76	51.88	7.51	0.04	36.21	1.62	0.49
Sample	Fiber analysis(dry)/%						
	Hemicellulose	Cellulose	Lignin	Extractable			
PR	19.56	53.20	18.96	8.28			
CR	17.71	39.45	27.62	15.22			

Note: ad, air dry free; d, dry free; daf, dry ash free; #, By difference.

Table 9. Physical properties and pore distribution of fresh Ni-Fe/HZSM-5 catalyst.

BET Surface Area (m ² /g)	t-Plot Micropore Area (m ² /g)	t-Plot External Surface Area (m ² /g)	Total Pore Volume (cm ³ /g)	Pore Size (nm)
219.50	133.02	84.48	0.17	3.11

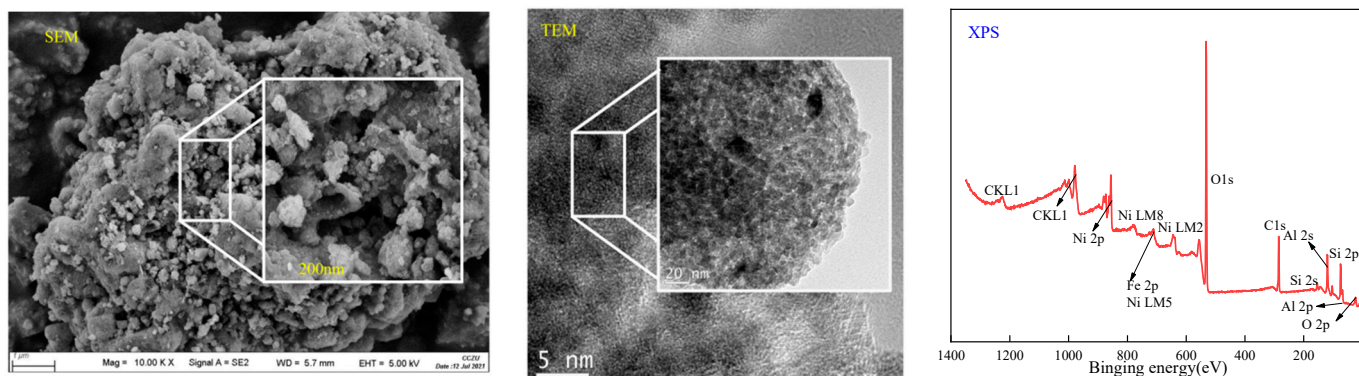


Figure 10. The morphology and crystalline-phase structure of fresh Ni-Fe/HZSM-5 catalyst.

3.2. Pyrolysis Method

3.2.1. Pyrolysis in TG

The thermogravimetric behavior of wood biomass was tested on a Pyris 1 TGA from PerkinElmer, Waltham, MA, USA. A total of 15 mg samples were uniformly spread in an alumina crucible to heat from ambient temperature to 100 °C at the rate of 10 °C/min for 1 h to remove free water. Then, non-isothermal thermogravimetric experiments were carried out in 99.999% helium (He) from 100 °C to 900 °C with heating rates of 10 °C/min, 20 °C/min, 30 °C/min, and 40 °C/min, respectively, to calculate apparent kinetic parameters. The terminal weight loss (wt.) and maximum weight loss rate temperature (T_m) were read from TG curves and DTG curves, respectively. The thermochemical properties of sam-

ples were analyzed by thermogravimetric experiment, and the characteristic temperature point was combined with the analysis of subsequent pyrolysis products.

3.2.2. Catalytic Pyrolysis in a Fixed Bed Reactor

Catalytic pyrolysis of wood biomass was carried out in a vertical quartz tubular reactor to further analyze the pyrolysis behavior and product evolution, and the reaction system is shown in Figure 11, which mainly includes pyrolysis reaction device, gas collection device, condensation and collection device of tar. Ni-Fe/HZSM-5 was used as catalyst with 5 g. Before the start of the experiment, 5 g Ni-Fe/HZSM-5 catalyst was evenly mixed with wood biomass samples and placed in the reaction tube. The gas–liquid separator was connected with the reactor at the bottom through ground glass by two levels of condensation with the ice water bath. Before the start of each experiment, 5 g samples were placed in the mid-reactor and heated to a set temperature at a heating rate of 10 °C/min and kept going for a while. N₂ was placed into the reactor at a flow rate of 90 mL/min for an inert environment and swept the high-temperature pyrolysis gas out. Pyrolysis gas was collected every 50 °C into sampling bags through the cooling system from 200 °C. Before sampling, the gas sampling bag shall be vacuumed and purified many times.

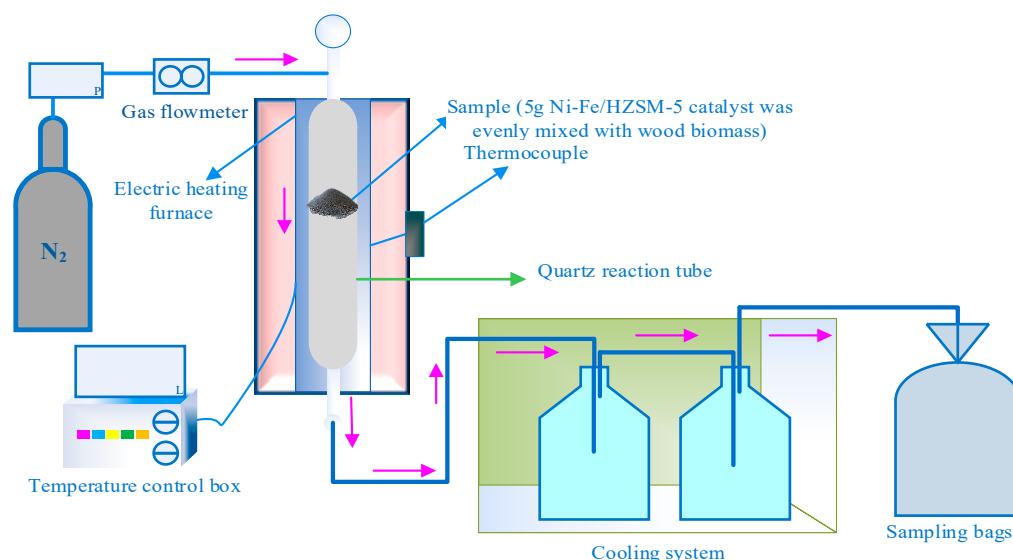


Figure 11. Primary high-temperature fixed bed reaction device.

3.3. Analysis of Samples and Products

3.3.1. Analysis of Pyrolysis Products

The gas products (H₂, CH₄, CO, and CO₂) were determined by gas chromatograph (Panna GC-A91), and the liquid products collected by the cooling system were analyzed by gas chromatography–mass spectrometer (GC-MS, Clarus 680-SQ 8 T, PerkinElmer, Waltham, MA, USA) with an Agilent DB-17MS capillary column, and the morphology characterized of solid products was by SEM. Determination of component content of gas by internal standard method, gas release rate, and yield were calculated by nitrogen balance method. The index parameters involved are calculated as follows:

$$\gamma_i = \frac{90 \times v_i}{v_{N_2} \times m_b} \quad (i = H, CH_4, CO, CO_2) \quad (11)$$

$$Y_i = \sum \gamma_i \times t \quad (12)$$

$$\text{Tar yield (\%)} = m_{\text{Tar}} \text{ (g)} / m_{\text{Biomass}} \text{ (g)} \times 100\% \quad (13)$$

$$\text{Char yield (\%)} = m_{\text{Char}} \text{ (g)} / m_{\text{Biomass}} \text{ (g)} \times 100\% \quad (14)$$

$$\text{Gas yield (\%)} = 1 - \text{Char yield (\%)} - \text{Tar yield (\%)} \quad (15)$$

$$\text{H conversion rate (\%)} = \left\{ \left[n_{(\text{H}_2)} + n_{(\text{CH}_4)} \right] / n_{\text{biomass-H}} \right\} \times 100\% \quad (16)$$

In Equation (11), γ_i is the release rate of gas i , mL/min; v_{N_2} is the flow of N_2 , 90 mL/min; v_i is the volume percentage of gas i (i represents H_2 , CH_4 , CO , CO_2), %; v_{N_2} is the volume percentage of N_2 in the tail gas from fixed bed reactor, %; m_b is the mass of biomass by dry and free ash basis. In Equation (12), Y_i is the yield of gas i , mL/g-biomass; t is the gas reception time, 5 min. In Equations (13)–(15), m_x is the quality of the x component (x represents tar, char, biomass), g. In Equation (16), $n(y)$ is the total H moles in the y fraction (y represents H_2 , CH_4 , biomass), mol.

3.3.2. Surface Characteristics of the Reacted Catalyst

The specific surface area, pore size, and pore volume of the reacted catalyst were measured by automatic specific surface area and porosity instrument (Tristar II 3020, MICRO cube, USA). Before the test, all the samples were treated in a high vacuum at 120 °C for 6 h. The specific surface area and pore size distribution of samples were measured by the N_2 adsorption method at liquid nitrogen temperature -196 °C, and the specific surface area was calculated by the crystal phase of the N_2 adsorption curve by the multi-point BET method, and the single-point pore volume at relative pressure $P/P_0 = 0.995$.

3.4. Apparent Kinetic Model

The visualization of reaction kinetics is the main research direction and also a general method to study the reaction kinetics of pyrolysis process of biomass in recent years. According to the law of mass action and Arrhenius equation, the kinetic relationship between reaction rate and reaction temperature was established. The kinetic parameters in the relationship were determined by thermogravimetric test data and the kinetic model to describe the reaction process. Usually, the kinetic analysis is the most severe stage of biomass weight loss; that is, the process of temperature drops from T_i to T_f . The sample with initial mass M_0 decomposes under programmed temperature. If the mass changes to m at a certain time, the decomposition rate can be expressed as shown in Equation (17) [46].

In Equation (17), E_a is the activation energy of the reaction, $\text{kJ}\cdot\text{mol}^{-1}$; A is frequency factor, min^{-1} ; T is the absolute temperature, K; β is the heating rate, °C/min; n is the reaction series. Most researchers approximately set the thermal decomposition of ligno-cellulosic materials as the first-order reaction [47,48], so $n = 1$. x is the conversion rate, %, which is defined as shown in Equation (18).

In Equation (18), m_0 , m_∞ , and m are the mass of the sample at initial, final, and time t , respectively, g. Take logarithms on both sides of the Equation (17), and the equation is expressed as shown in Equation (19).

$$\frac{dx}{dT} = \frac{A}{\beta} \exp\left(-\frac{E_a}{RT}\right) (1-x)^n \quad (17)$$

$$x = \frac{m_0 - m}{m_0 - m_\infty} \quad (18)$$

$$\ln\left(\frac{dx}{dT}\right) - n \ln(1-x) = \ln\left(\frac{A}{\beta}\right) - \frac{E_a}{RT} \quad (19)$$

Thus, there is a linear relationship between the left side of Equation (19) and $1/T$; the form is $Y = ax + b$ form, the line slope is $-E_a/R$ and the intercept is $\ln(A/\beta)$.

Finally, the main reaction section of pyrolysis is analyzed and calculated according to the Equation (19) and combined with the data of TG/DTG. The kinetic parameters of pyrolysis process of biomass are obtained. Then, the reaction kinetic model can be established by Equation (17), and the kinetics of pyrolysis process of biomass was analyzed.

4. Conclusions

The apparent kinetic of PR and CR was investigated under four diverse heating rates by TG/DTG. Both PR and CR exhibited three consecutive stages of weight loss and the TG/DTG curves. The characteristic parameters shifted to a higher temperature as the heating rate rose. The activation energies and preexponential factor obtained from the law of mass action and Arrhenius equation for CR were 72.38 kJ/mol and 1147.11 min^{-1} and located in 72.36 kJ/mol and 1144.36 min^{-1} for PR. The pyrolysis mechanisms of wood biomass were mainly the process of carbon enrichment and depolarity functional group of organic components. H_2 was the most dominant gaseous product during the pyrolysis process, followed by C–O bond-containing species (CO , CO_2), while CH_4 was abundant in pyrolysis gas. The high temperature was beneficial for promoting the pyrolysis of biomass, increasing pyrolysis gas yield, and reducing tar yield. In the presence of the Ni-Fe/HZSM-5 catalyst, the gas yield significantly increased to $117.9 \text{ mL/g-biomass}$ at the pyrolysis temperature of 700°C . The catalytic pyrolysis of MWC could generate larger amounts of oxygenated product. In particular, more hydrocarbons like AL, AC, ALc, KE, PH, FU, and ES were observed in the liquid products. Furthermore, the H_2O steam had more effect on the product evolution and yield of gaseous products. However, too much H_2O inhibits the cracking/reforming reaction of tar and also consumes a lot of energy. In particular, the gas yield and hydrogen conversion were 76.94% and 15.90%, and the H_2/CO was 2.07 under the H_2O steam flow rate of 1 mL/min. The yields of H_2 , CO , and CO_2 were $107.35 \text{ mL/g-biomass}$, $53.70 \text{ mL/g-biomass}$, and $99.31 \text{ mL/g-biomass}$, respectively. The pyrolysis mechanism and product distribution of wood biomass were demonstrated through different indexes. It was concluded that wood biomass has great advantages in pyrolysis for producing hydrogen-rich gas, and it has a good application prospect as the raw material of alternative fuel. However, understanding how to carry out deep purification and the efficient utilization of high-temperature pyrolysis gas is an important direction for promoting the development of biomass technology.

Supplementary Materials: The following supporting information can be downloaded at: <https://www.mdpi.com/article/10.3390/catal14030200/s1>, Table S1. Numbers of liquid products.

Author Contributions: Conceptualization, Y.W. and T.L.; methodology, X.L.; software, X.L. and T.H.; validation, Y.L.; formal analysis, X.L. and P.L.; investigation, X.L. and Z.C.; resources, Y.W., T.L. and P.L.; data curation, X.L. and Z.W.; writing—original draft preparation, X.L. and P.L.; writing—review and editing, Y.W. and T.L.; visualization, X.L. and P.L.; supervision, Y.W. and T.L.; funding acquisition, T.L., P.L. and Z.C. All authors have read and agreed to the published version of the manuscript.

Funding: This study was funded by the National Key R&D Program of China (2022YFB4201901), a Special scientific research project for civil aircraft in 2020-EU China Sustainable Aviation Fuel (MJ-2020-D-09), Changzhou Sci & Tech Program (CE20222034, CJ20220246 and CJ20220138), and Key R&D Program Project in Henan Province (Soft Science) (232400411019).

Data Availability Statement: The data presented in this study are available upon request from the corresponding author.

Conflicts of Interest: The authors declare no conflicts of interest.

References

1. Su, J.; Li, T.; Luo, G.; Zhang, Y.; Naranov, E.R.; Wang, K. Co-hydrolysis of pine and HDPE over bimetallic catalysts: Efficient BTEX production and process mechanism analysis. *Fuel Process. Technol.* **2024**, *249*, 107845. [CrossRef]
2. Cai, J.; Lin, N.; Li, Y.; Xue, J.; Li, F.; Wei, L.; Yu, M.; Zha, X.; Li, W. Research on the application of catalytic materials in biomass pyrolysis. *J. Anal. Appl. Pyrolysis* **2024**, *177*, 106321. [CrossRef]
3. Suriapparao, D.V.; Tejasvi, R. A review on role of process parameters on pyrolysis of biomass and plastics: Present scope and future opportunities in conventional and microwave-assisted pyrolysis technologies. *Process Saf. Environ. Prot.* **2022**, *162*, 435–462. [CrossRef]
4. Wang, W.; Luo, G.; Zhao, Y.; Tang, Y.; Wang, K.; Li, X.; Xu, Y. Kinetic and thermodynamic analyses of co-pyrolysis of pine wood and polyethylene plastic based on Fraser-Suzuki deconvolution procedure. *Fuel* **2022**, *322*, 124200. [CrossRef]

5. Tan, H.; Yang, M.; Chen, Y.; Chen, X.; Fantozzi, F.; Bartocci, P.; Tschentscher, R.; Barontini, F.; Yang, H.; Chen, H. Preparation of aromatic hydrocarbons from catalytic pyrolysis of digestate. *Chin. J. Chem. Eng.* **2023**, *57*, 1–9. [[CrossRef](#)]
6. Wrasman, C.J.; Wilson, A.N.; Mante, O.D.; Lisa, K.; Dutta, A.; Talmadge, M.S.; Dayton, D.C.; Uppili, S.; Watson, M.J.; Xu, X.; et al. Catalytic pyrolysis as a platform technology for supporting the circular carbon economy. *Nat. Catal.* **2023**, *6*, 563–573. [[CrossRef](#)]
7. Wang, S.; Cheng, A.; Liu, F.; Zhang, J.; Xia, T.; Zeng, X.; Fan, W.; Zhang, Y. Catalytic conversion network for lignocellulosic biomass valorization: A panoramic view. *Ind. Chem. Mater.* **2023**, *1*, 188–206. [[CrossRef](#)]
8. Ranzi, E.; Cuoci, A.; Faravelli, T.; Frassoldati, A.; Migliavacca, G.; Pierucci, S.; Sommariva, S. Chemical Kinetics of Biomass Pyrolysis. *Energy Fuels* **2008**, *22*, 4292–4300. [[CrossRef](#)]
9. Wang, G.; Dai, Y.; Yang, H.; Xiong, Q.; Wang, K.; Zhou, J.; Li, Y.; Wang, S. A Review of Recent Advances in Biomass Pyrolysis. *Energy Fuels* **2020**, *34*, 15557–15578. [[CrossRef](#)]
10. Singh, S.; Chakraborty, J.P.; Mondal, M.K. Intrinsic kinetics, thermodynamic parameters and reaction mechanism of non-isothermal degradation of torrefied *Acacia nilotica* using isoconversional methods. *Fuel* **2020**, *259*, 116263. [[CrossRef](#)]
11. Jaffar, M.M.; Nahil, M.A.; Williams, P.T. Pyrolysis-catalytic hydrogenation of cellulose-hemicellulose-lignin and biomass agricultural wastes for synthetic natural gas production. *J. Anal. Appl. Pyrolysis* **2020**, *145*, 104753. [[CrossRef](#)]
12. Das, P.; Tiwari, P. Thermal degradation kinetics of plastics and model selection. *Thermochim. Acta* **2017**, *654*, 191–202. [[CrossRef](#)]
13. Mishra, G.; Kumar, J.; Bhaskar, T. Kinetic studies on the pyrolysis of pinewood. *Bioresour Technol.* **2015**, *182*, 282–288. [[CrossRef](#)]
14. Hosoya, T.; Kawamoto, H.; Saka, S. Cellulose–hemicellulose and cellulose–lignin interactions in wood pyrolysis at gasification temperature. *J. Anal. Appl. Pyrolysis* **2007**, *80*, 118–125. [[CrossRef](#)]
15. Xu, M. Study on the Characteristics Analysis and Experimental of Biomass Pyrolysis and Gasification. Master’s Thesis, Tianjin University, Tianjin, China, 2008.
16. Xiu, S.; Yi, W.; He, F. Analysis on Thermogrametric Curves of Biomass. *J. Zibo University (Nat. Sci. Eng. Ed.)* **2002**, *2*, 82–85.
17. Jiang, J.; Shen, Y. Study on Reaction Kinetics of Biomass Pyrolysis. *Chem. Ind. For. Prod.* **2003**, *23*, 1–6.
18. Zhang, C. Study on Pyrolysis and its Reaction Kinetics of Agricultural and Forestry Biomass. Master’s Thesis, Beijing University of Chemical Technology, Beijing, China, 2013.
19. Yao, Q.; Xu, L.; Zhang, Y. Production of High Value-added Chemicals by Catalytic Fast Pyrolysis of Biomass. *Chem. Ind. For. Prod.* **2015**, *35*, 138–144.
20. Wu, H.; Liu, A.; Li, L.; Wang, X.; Zhang, Z.; Li, H.; He, F. Effects of potassium on pyrolysis characteristics of pine. *J. Fuel Chem. Technol.* **2014**, *42*, 7.
21. Chen, W.; Lu, J.; Yang, M.; Li, J.; Sun, J. Characteristics of Purolysis Products of Typical Biomass at Different Temperatures. *Ind. Heat.* **2019**, *48*, 6.
22. Sun, T. Production Distribution and Experimental Study of Lignocellulosic Biomass Directional Pyrolysis. Ph.D. Thesis, Henan Agricultural University, Zhengzhou, China, 2021.
23. Dickerson, T.; Soria, J. Catalytic Fast Pyrolysis: A Review. *Energies* **2013**, *6*, 514–538. [[CrossRef](#)]
24. Duan, D.; Wang, Y.; Dai, L.; Ruan, R.; Zhao, Y.; Fan, L.; Tayier, M.; Liu, Y. Ex-situ catalytic co-pyrolysis of lignin and polypropylene to upgrade bio-oil quality by microwave heating. *Bioresour. Technol.* **2017**, *241*, 207–213. [[CrossRef](#)]
25. Wang, Y.; Akbarzadeh, A.; Chong, L.; Du, J.; Tahir, N.; Awasthi, M.K. Catalytic pyrolysis of lignocellulosic biomass for bio-oil production: A review. *Chemosphere* **2022**, *297*, 134181. [[CrossRef](#)]
26. Qiu, B.; Tao, X.; Wang, J.; Liu, Y.; Li, S.; Chu, H. Research progress in the preparation of high-quality liquid fuels and chemicals by catalytic pyrolysis of biomass: A review. *Energy Convers. Manag.* **2022**, *261*, 115647. [[CrossRef](#)]
27. Liao, Y. Hydrogen-Rich Gas Production from Biomass Catalytic Gasification over Fe-Ce/Olivine Catalyst. Master’s Thesis, Huazhong University of Science and Technology, Wuhan, China, 2015.
28. Zhang, X.; Chen, G.; Meng, X.; Li, X. Production of hydrogen-rich gas from biomass by catalytic pyrolysis. *J. Fuel Chem. Technol.* **2004**, *32*, 446–449.
29. Feng, J.; Shu, X. Study on Preparation of Hydrogen from Biomass Waste. *Environ. Sustain. Dev.* **2007**, *4*, 234–237.
30. Hu, G. Research on biomass gasification catalysts for hydrogen production. Master’s Thesis, Dalian University of Technology, Dalian, China, 2005.
31. Pang, Y.; Meng, H.; Chen, Y.; Liu, X.; Wu, Y. Biomass charcoal catalytic with Ca/Fe enhancing hydrogen production by pyrolysis volatile steam reforming. *Trans. Chin. Soc. Agric. Eng.* **2019**, *35*, 187–192.
32. Cao, Z.; Wang, L.; Wu, Y.; Zhu, Y. Research progress in effect of catalysts on hydrogen production by biomass gasification. *Mod. Chem. Ind.* **2021**, *41*, 47–52.
33. Hao, Q.; Wang, C.; Lu, D.; Wang, Y.; Li, D.; Li, G. Production of hydrogen-rich gas from plant biomass by catalytic pyrolysis at low temperature. *Int. J. Hydrog. Energy* **2010**, *35*, 8884–8890.
34. Fernandez, E.; Amutio, M.; Artetxe, M.; Arregi, A.; Santamaria, L.; Lopez, G.; Bilbao, J.; Olazar, M. Assessment of product yields and catalyst deactivation in fixed and fluidized bed reactors in the steam reforming of biomass pyrolysis volatiles. *Trans. Inst. Chem. Eng. Process Saf. Environ. Prot. Part B* **2021**, *145*, 52–62. [[CrossRef](#)]
35. Sun, N.; Ying, H.; Xu, W.; Sun, Y.; Xu, Y.; Jia, S. Catalytic gasification of pine sawdust for producing hydrogen-rich gas. *Chem. Ind. Eng. Prog.* **2017**, *36*, 2158–2163.

36. Ghodke, P.K.; Sharma, A.K.; Jayaseelan, A.; Gopinath, K.P. Hydrogen-rich syngas production from the lignocellulosic biomass by catalytic gasification: A state of art review on advance technologies, economic challenges, and future prospectus. *Fuel* **2023**, *342*, 127800. [[CrossRef](#)]
37. Collard, F.-X.; Blin, J.; Bensakhria, A.; Valette, J. Influence of impregnated metal on the pyrolysis conversion of biomass constituents. *J. Anal. Appl. Pyrolysis* **2012**, *95*, 213–226. [[CrossRef](#)]
38. Zhou, X.; Zhang, L.; Chen, Q.; Xiao, X.; Wang, T.; Cheng, S.; Li, J. Study on the mechanism and reaction characteristics of red-mud-catalyzed pyrolysis of corn stover. *Fuel* **2023**, *338*, 127290. [[CrossRef](#)]
39. Lu, Q.; Zhang, T.; Deng, X.; He, R.; Yuan, S.; Li, J.; Xie, X.; Li, W.; Liu, Z.; Zhang, X. Enhancement of gas and aromatics by in-situ catalytic pyrolysis of biomass in the presence of silica gel. *Biomass Bioenergy* **2020**, *138*, 105567. [[CrossRef](#)]
40. Xia, S.; Yang, H.; Lu, W.; Cai, N.; Xiao, H.; Chen, X.; Chen, Y.; Wang, X.; Wang, S.; Wu, P.; et al. Fe–Co based synergistic catalytic graphitization of biomass: Influence of the catalyst type and the pyrolytic temperature. *Energy* **2022**, *239*, 122262. [[CrossRef](#)]
41. Tsaplin, D.; Sadovnikov, A.; Ramazanov, D.; Gorbunov, D.; Ryleeva, V.; Maximov, A.; Wang, K.; Naranov, E. Selective Hydrodeoxygenation of Guaiacol to Cyclohexane over Ru-Catalysts Based on MFI Nanosheets. *Micro* **2023**, *3*, 610–619. [[CrossRef](#)]
42. Liu, P.; Wang, Y.; Zhou, Z.; Yuan, H.; Zheng, T.; Chen, Y. Effect of carbon structure on hydrogen release derived from different biomass pyrolysis. *Fuel* **2020**, *271*, 117638. [[CrossRef](#)]
43. Liu, P.; Liu, L.; Zhou, Z.; Li, Y.; Yuan, H.; Huhetaoli; Lei, T. Co-pyrolysis of pine sawdust with aluminum dross for immobilization of heavy metal and enhancing hydrogen generation. *Fuel* **2021**, *305*, 121597. [[CrossRef](#)]
44. Liu, P.; Lang, P.; Chen, Z.; Li, Y.; Sun, T.; Yang, Y.; Huhe, T.; Lei, T. Relevance of chemical structure in different wood wastes to pyrolysis behavior: Kinetics and hydrogen release. *J. Energy Inst.* **2023**, *111*, 101416. [[CrossRef](#)]
45. Li, X.; Liu, P.; Yang, Y.; Li, Y.; Wu, S.; Huhe, T.; Huang, S.; Sun, T.; Wang, L.; Wu, Y.; et al. Pyrolysis behaviors of biomass tar-related model compounds catalyzed by Ni-modified HZSM-5 molecular sieve. *Ind. Crops Prod.* **2023**, *199*, 116743. [[CrossRef](#)]
46. Lang, P.; Liu, P.; Li, Y.; Li, X.; Lei, T. Study on Kinetics and Thermodynamic Parameters for Pyrolysis of Different Sawdust Biomass. *China For. Prod. Ind.* **2022**, *59*, 30–37+52.
47. Sun, L. Mechanism and Experiment of Biomass Pyrolysis for Hydrogen Production. Ph.D. Thesis, Tianjin University, Tianjin, China, 2007.
48. Lan, Y.; Lv, M.; Ma, C.; Shi, M. Study on the Characteristics and Dynamics of Pyrolysis Process Agricultural Residues. *Acta Energetica Solaris Sin.* **2002**, *23*, 203–206.

Disclaimer/Publisher’s Note: The statements, opinions and data contained in all publications are solely those of the individual author(s) and contributor(s) and not of MDPI and/or the editor(s). MDPI and/or the editor(s) disclaim responsibility for any injury to people or property resulting from any ideas, methods, instructions or products referred to in the content.